Consumable electrode vacuum arc remelting of gamma-TiAl with online feeding

Alexander Specht; Bernd Friedrich

Institute and Chair for Process Metallurgy and Metal Recycling at RWTH Aachen University, Aachen, Germany

e-mail: ASpecht@ime-aachen.de

Abstract. Vacuum arc remelting is widely recognized for its ability to produce high quality ingots for demanding applications. Since its introduction in the 1940s, great efforts have been undertaken to increase productivity, reliability and furnace safety by different iterations of furnace design accompanied by improvements in process data acquisition and interpretation to allow remelting behaviour simulation. However, essential challenges regarding the heat extraction remain to this day, due to the direct coupling of melt rate, melt power, gap distance, furnace geometry, cooling capabilities and physical properties of the material when using a conventional vacuum arc remelting setup with consumable electrode. These parameters define achievable temperature gradients and heat transfer limits in the system, thus dictate the microstructure formation as well as segregation effects. To overcome these limitations, a novel approach is introduced at IME RWTH University, which uses a continuous online feeding of same sort metal powder into the melt pool during the remelting process, to increase heat extraction and nucleation density. In this study the successful introduction of metal powder into the pool via online feeding during vacuum arc remelting with consumable electrode is presented together with its influence on the process behaviour and remelting result.

1. Introduction

Consumable electrode vacuum arc remelting (VAR) is a well-established final melt refinement step for commercially pure titanium, titanium- and nickel-based alloys as well as for refractory metals and their alloys, increasing their chemical and microstructural homogeneity, while decreasing the number of light non-metallic inclusions (NMI's). The main influencing factors on the remelting process and therefore product quality are the supplied melt power, melt rate, arc gap length in between pool and electrode tip and crucible coil current, which are all in a complex link. The challenge of these complex technical connections is met by manufacturers of high-performance alloys and furnace equipment, that work towards a more stable, reliable and near defect free remelting process through furnace setup optimization as well as optimized remelting recipes and electrode conditioning.

In preparation of this work, patent research has been undergone to show areas of development pursued by relevant furnace equipment manufacturers and/or producers of VAR material. The patents are classified, subdivided in three the three groups "Furnace Equipment" (yellow), "Process Control" (blue) and "Special Remelting Techniques" (green) and represented in form of a pie chart, as seen in Figure 1. Although approximately three quarters of the examined patents deal with material specific remelting techniques and control mechanisms, none of the presented solutions are able to resolve the direct coupling of the melt rate with the solidification rate. This coupling is not an issue for all applications,

but limits remelting if heat conductivity of the remolten material is low, thermal resistance between ingot and crucible wall is high or ingot diameter is large. The listed limiting factors are met for example in large diameter titanium ingot remelting. To prevent the formation of a deep melt pool, the melt rate has to be continuously decreased over the time of the main remelting phase as it is described for example in the patents by Xiaohua et al. [1] and Huang Shuo et al. [2]. Although the decrease in melt rate resolves the issue of pool depth control, it causes a loss in productivity and may be unfeasible if melt rate cannot be reduced for technical reasons.

The presented study investigates the continuous addition of metal powder into the melt pool during VAR. The addition of granular material into a liquid melt pool with the goal of alloying has been described in a patent by Spaniol et al. [3] for the production of a Nb3Sn-alloy and in an expired patent from Schuyler et al. [4] for the production of refractory metal ingots from granular material. Other than these there are no patents or other publications regarding consumable electrode VAR with online feeding to the authors knowledge. The study therefore aims to build on these approaches and introduces the continuous addition of metal powder, as a new pool depth control mechanism for consumable electrode VAR. High-grade scrap from additive manufacturing was continuously fed during the remelt in order to cool down the melt pool, whilst maintaining constant energy input and therefore not decreasing furnace productivity. This first approach study demonstrates the feasibility and potential of continuous powder addition for microstructure manipulation as well as for alloying purposes.

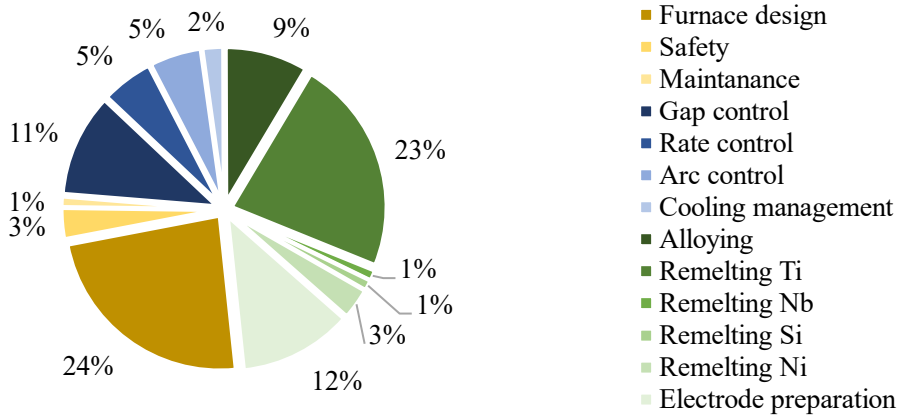

Figure 1: Patents regarding VAR process and furnace in the thematic areas of groups “Furnace Equipment” (yellow), “Process Control” (blue) and “Special Remelting Techniques” (green). [1, 3–95]

2. Experiments

In this study gamma-TiAl alloy powder scrap from production is fed during remelting of either virgin material compacted electrodes or sound metal ingots from a VAR remelt to identify mixing behaviour and the impact of continuous feeding on remelting process. The trials were conducted in a Vacuum Arc Remelter “VAR L 200” with a vibro-feeder module from ALD vacuum technologies GmbH with a 200 mm diameter crucible. The furnace setup is represented in Figure 2. In addition to the process data acquisition integrated into the furnace control, an infrared thermal imager and high-resolution optical imager are aimed at the pool from the top. The viewports for the observation are covered by toughened safety glass for vacuum tightness, which itself is protected from liquid melt droplets and sputtering by another pane of quartz glass. Both glasses are of high optical quality and transparent for the visible spectrum as well as infrared radiation at the observed wavelength of 0.8 – 1.1 µm. Data from the imagers is recorded on one PC, furnace operating interface and furnace data acquisition is performed by a second PC, facilitating clock synchronization between all continuous measurements.

The fed powder is a gamma-TiAl alloy powder particle size fraction larger than 180 µm (Alloy Ti48Al2Cr2Nb) from sieving after powder production via electrode induction melting inert gas atomization (EIGA). Because online feeding during remelting poses a novelty for the VAR process and operation safety has highest priority, two scenarios were investigated. In scenario A material is fed into

the pool in small packages of approx. 10 g during the main remelting phase of a primary remelt electrode from compacted virgin material at minimal power input to avoid side arcing and get first experience of remelting behaviour. The TiAl powder is mixed with Fe powder of 99 % purity and packed in commercial Al-foil cuttings of 5x5 cm to avoid melt contamination with other elements. Fe acts as a tracer element, since it is well soluble in the alloy and easy to detect via X-ray fluorescence analysis (XRF) on cut samples which allows the observation of the powder distribution in the melt pool. The compacted electrode has a polygonal cross-section and is relatively thin with a round reference diameter of approx. 110 mm in the 200 mm diameter crucible. This ratio was chosen to allow plenty of space between the crucible wall and electrode for the powder packages to fall through the anulus and to ensure the elimination of potential side arcs. On the downside, the setup with an electrode this thin does not represent a process with comparable to an industrial case with regard to the relation between the heat transfer from the electrode to the pool and the heat extraction via the crucible.

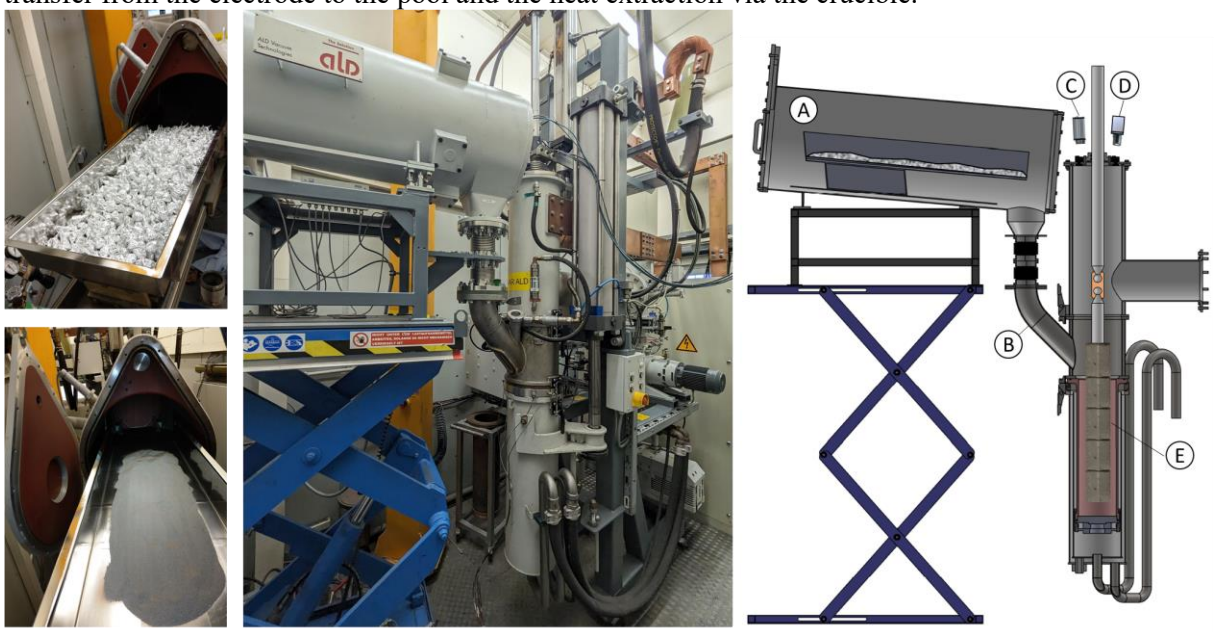

Figure 2: Feeder tray with powder packages (top left), feeder tray with loose powder (bottom left) and VAR furnace with vibro-feeder at IME RWTH Aachen (middle) with a cross section schematic showing the furnace with the vibro-feeder-tray (A) connected via the connector (B) as well as the positioning of the IR-imager (C) and high-resolution optical imager (D) facing the anulus between crucible and electrode (E).

For this reason, in scenario B a setup closer to industrial application was chosen, where loose powder is fed into the remelting process of a sound electrode with a round profile at a diameter of 160 mm. The reference trial electrode consists of three and the electrode with feeding of two ingots from prior VAR remelting with a diameter of approx. 160 mm. Ingots are trimmed at both ends, turned upside down and welded together. Other than in scenario A remelting temperature is continuously monitored via IR and high resolution (HR) imager. All mayor differences between the two setups are sown in Table 1.
The remelting trials comprise furnace assembly, furnace evacuation, Ar-flushing with technical Ar 4.8, process start and main melting phase with material feeding under a stabilizing coil current of 5-10 A at altering polarity of 1 Hz. Feeding of loose powder was done in intervals of 3 mins with breaks in between to allow clear visibility onto the pool surface without interference by the powder in the anulus for purposes of IR-imager calibration. At process end power is cut without hot topping. The following remelting parameters are logged with a frequency of 1 Hz: electrode weight, melt rate, melt current, voltage, drips, electrode position, cooling water temperature in an out, furnace pressure, electrode drive speed, electrode position, stabilizing coil current, feeder weight and feeder feed rate. From these values, crucible dimensions and the physical properties of the remolten material, the ingot height, the electrode length and arc gap were calculated for every dataset during remelting.

Table 1: Main differences in the trial setups for the two tested scenarios

	Scenario A	Scenario B
Electrode Composition	compacted virgin material electrode	sound material from 2 - 3 previous VAR remelts
Electrode Diameter	110 mm	160 mm
Fed Material	0 - 17 wt.% of remolten ingot mass is Ti48Al2Cr2Nb-powder in packets	3 wt.% of remolten ingot mass is loose Ti48Al2Cr2Nb-powder
Ingot Weight	approx. 15 kg	approx. 40 kg
Melt Current	1.5 kA	2.6 kA
Analytics	Furnace data, XRF mapping, Macrostructure	Furnace data, XRF mapping, Macrostructure, IR&HR Images

The HR optical camera is set to an exposure time of 800 to 2500 µs at manual varied aperture opening to compensate for changes in brightness. Images are captured at a rate of 25 Hz and converted to video format. The infrared imager captures images at 50 Hz in raw format. IR raw data is evaluated for the pool temperature determination as described by Specht et al. [96].
In addition to the temperature evaluation for mean pool temperature through the determination of the correct maximum in the bimodal distribution at emissivity ε=0.38 and transmissivity τ=0.67, an approximation for the electrode underside surface is calculated. Due to the high reflectance of the liquid metal surfaces the temperature is calculated from a corrected emissivity under the assumption that the angle of observation, temperature dependence of ε and dissipation of radiation is small. Under these circumstances the emissivity of the electrode ε_e is assumed to be equal to the emissivity of the pool ε_p plus the reflected radiation from the electrode underside as shown in Eq. 1.

$$\varepsilon_e = \varepsilon_p + \varepsilon_p * (1 - \varepsilon_p) \qquad \text{Eq. 1}$$

The raw data is re-evaluated using the adapted values of ε=0.6158 and τ=0.67. The resulting histogram in Figure 3 shows an exemplary bimodal distribution of temperature values for the electrode and pool evaluation. For a temperature plot over time, a histogram for 10 seconds (4000 values) each is evaluated regarding its peaks, giving out a mean electrode underside and pool temperature for every point in time during remelting.
After the process end, the ingots were cooled in the crucible under 200 mbar Ar for approx. 2 h. The extracted ingots were cut in half along the centre axis, analysed via X-ray fluorescence analysis (XRF) in a grid patten, every 2 cm in height at 1 cm and 5.5 cm from the surface, as well as on the centre axis. The cutting face is then polished down to 1000 grit and etched with a solution of 18.5 % HCl in distilled water for 2.75 h.

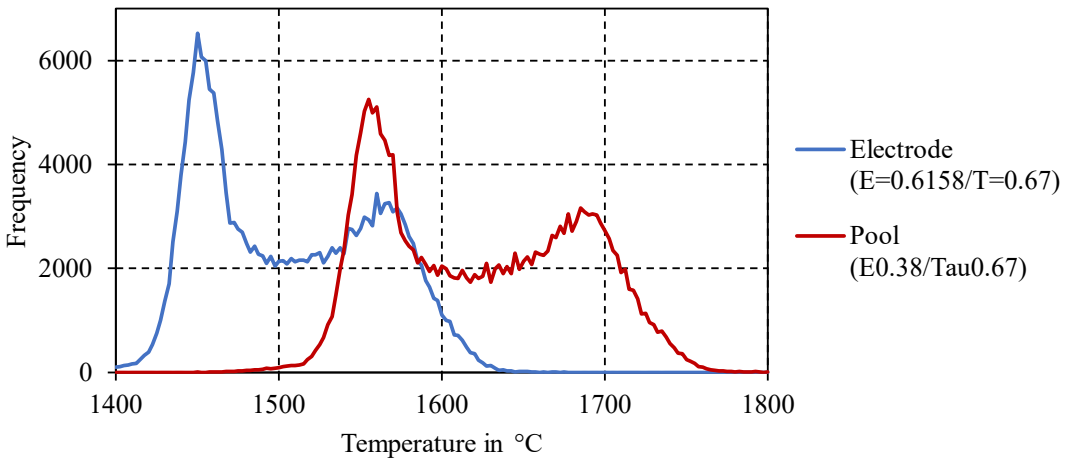

Figure 3: Histogram for the two evaluated emissivity values for the pool and the electrode underside over a time of 10 minutes with a bin width of 2.5 °C.

3. Results and discussion

The remelting with feeding of packages was successfully performed and package distribution over the pool surface was observed to be equal in the camera images. The feed material appeared to have an influence on furnace implemented process control function for electrode feed control. As a result, manual control on the basis of constant electrode speed and arc current was chosen for trials in scenario A. The melting behaviour of packages has been identified to be dependent on pool condition. If the temperature in the pool and pool depth were insufficient, a package touching the melt surface created a powder heap which did not dissolve or disperse by the bath movement. It was observed that existing heaps attracted arcs but did not cause a constricted arc or a strong deviation from the usual diffusive arc mode. Furthermore, side arcs or glow discharge was not detected as a result of the material feeding.

The dissolution behaviour of the powder packages in scenario A indicates limitations with regard to the maximum amount of fed powder and the ability of the VAR to cope with fed material if it is clustered or agglomerated when reaching pool surface. Those areas are identified in the cross-section cuts of the ingots shown in Figure 4, as porosity clusters and/or uneven ingot surfaces and cracks. The macrostructure of both ingots shows a darker bottom zone with needle like grains, which is comparable for both ingots. Above that lays the area of residual solidification for the ingot without feeding, showing large grains associated with a slower cooling. In the ingot with feeding there is close to no difference between the upper and the lower part, showing needle like grains with little ordered solidification direction and small spots of porosity. The pores may either stem from aforementioned clustered powder residue or solidification cavitation due to rapid local solidification. The difference in the solidification behaviour in the upper part of the ingot is interpreted as a result of the combined effect of increased nucleation density and decreased pool temperature.

The XRF-mapping showed Fe content varying between 0.3 and 0.4 wt.% corresponding to a powder content of 14 and 18 wt.% with an average concentration of 16 wt.% in the main metal matrix over the whole diameter. Areas of undissolved powder heaps showed Fe contents of up to 0.75 wt% corresponding to 70 wt.% powder contents. Overall, these results show promising behaviour, where transport mechanisms through convection and diffusion in the pool are fast enough to reach fair chemical homogeneity, even in scenarios of power addition which creates solidification defects.

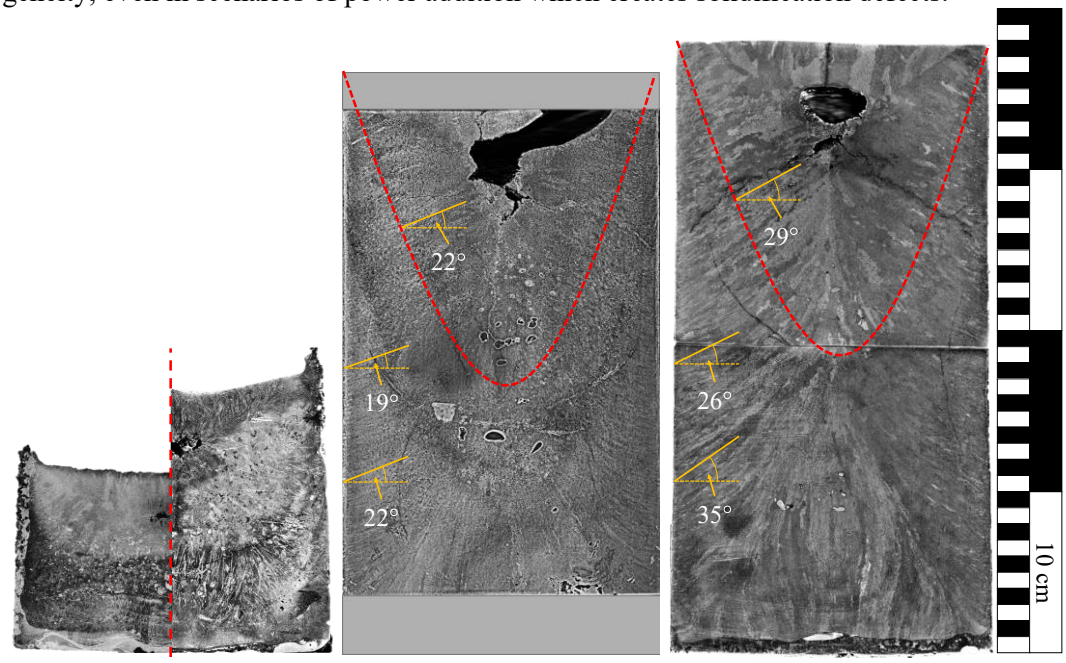

Figure 4: Ingot cross section cut after macro etching. Left: half ingots each from scenario A without feeding (left half) and with 17 wt.% powder feeding (right half). Middle: Ingot from scenario B without feeding. Grey areas on top and bottom of the ingot represent cut away parts. Right: Ingot from scenario B with 3 wt.% feeding. In the two images of the ingots from Scenario B pool depth at power shut down (red) and grain orientation relative to horizon (orange) are marked.

The remelting of pre-molten, sound metal electrodes proved to be more stable when compared to the virgin material but showed an expected increase in melt rate towards the end of one and a sudden decrease in melt rate at the beginning of the next electrode part as seen in Figure 5. Since the parts of the electrode are joined by a surficial weld, the remaining gap in between the two parts creates a heat barrier. This causes the faster melting of the remaining part preceding the shift from one part to the next at the time of 0:35 h:mm. The temperature at the electrode underside shows a decrease of about 30 °C during the time before complete consumption which is explained by the increased bulk-temperature which decreases the needed superheating at the electrode underside. After the consumption of the first part the remaining part needs to pre-heat before it enters regular remelting. This is accompanied by a decrease in mayor drip shorts visualized in the voltage signal. Even though the remelting parameters return to normal over the course of the next three minutes, the effect of the horizontal gap in the electrode is very visible in the macro etching at 12 – 16 cm ingot height for the ingot without feeding and 9 – 11 cm ingot height for the ingot with feeding. In both etchings particles can be found at the ingot centre at the height of the expected pool bottom position during the transition. The defects are therefore expected to be a result of the inconsistent remelting conditions and not the powder addition. Another set of defects are found at the bottom of the final pool. Their appearance is linked to a similar discontinuity in solidification conditions, due to the lack of a hot topping after main melting phase.

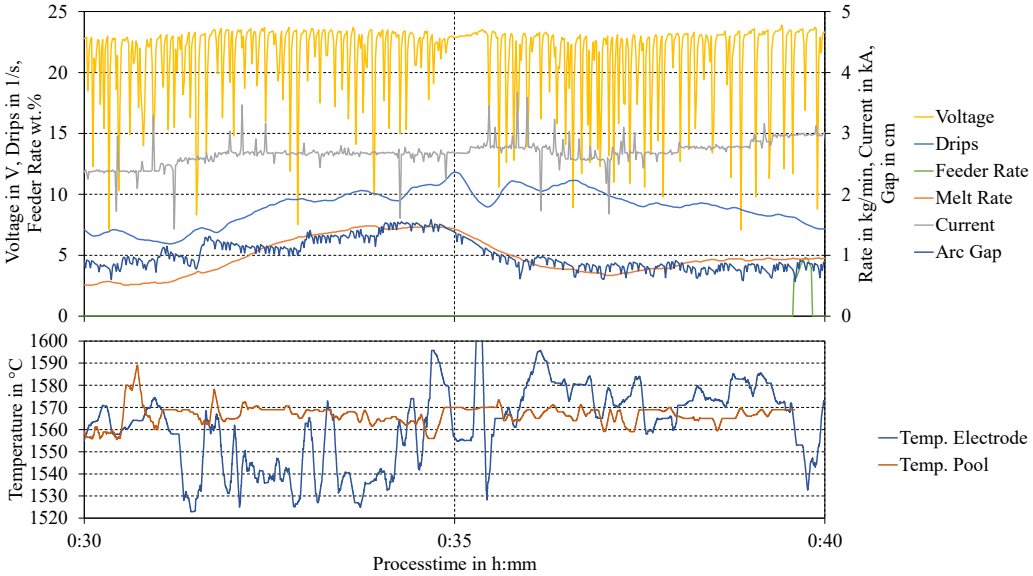

Figure 5: Excerpt of melt protocol (top) and temperatures from IR imager (bottom) for the remelting trial with loose powder feeding in scenario B during the transition from one pre molten part of the electrode to the next.

The remelting with the addition of loose powder in scenario B showed a stabilizing effect on the arc resulting in a behaviour observed through optical observation of arc mode and voltage data, similar to a remelt without powder feeding and the use of a stabilizing crucible coil current. A possible cause for this behaviour could be the surficial cooling effect of the powder, that comes into contact with the pool in the anulus area first, leaving the area under the electrode as main area of ions for arc plasma generation. Negative impact on the remelting parameters were observed neither in the camera images nor the remelting parameters shown in Figure 6. The powder particles were observed to be evenly distributed over the pool surface as they fall in. floating particles got pushed out towards the crucible wall, forming ribbons of powder materials that get ripped apart and reform repeatedly by the wave motions on the pool surface. The build-up of a thicker shell area at the crucible walls or other undesirable behaviour is not observed and both ingots show a sound cross section without porosity. The solidification direction of the columnar crystals is oriented diagonally inwards and up towards the top for both ingots. The angle of orientation measured from horizontal reference is significantly shallower for the reference trial without feeding when compared with the trial with powder addition during main melting phase and in the residual solidification at process end.

The steeper grain orientation indicates a lower overall pool temperature during the remelting and final solidification with addition of metal powder. This assumption is backed by the temperature evaluation via IR-thermography that shows an overall lower temperature for the trial with feeding, when compared to the reference trial. A further distinguishing feature is the difference between pool and electrode underside temperature in the two setups. Where the temperature at the electrode underside lies about 10 °C above that of the pool during the reference trial, there is close to no distinct difference between the two temperatures in the trial with powder addition. The largest difference between the two setups is therefore found in the electrode underside temperature. This phenomenon might result from a higher than usual anode sided energy input, caused by powder on the pool surface. An anode effect of that kind would explain the higher relative heat input into the pool and the overall lower temperature at comparable energy input. This theory is based on the IR measurements of these two non-replicated remelting trials. It seems plausible in the context of furnace data and macrostructural images but cannot be confirmed without further testing.

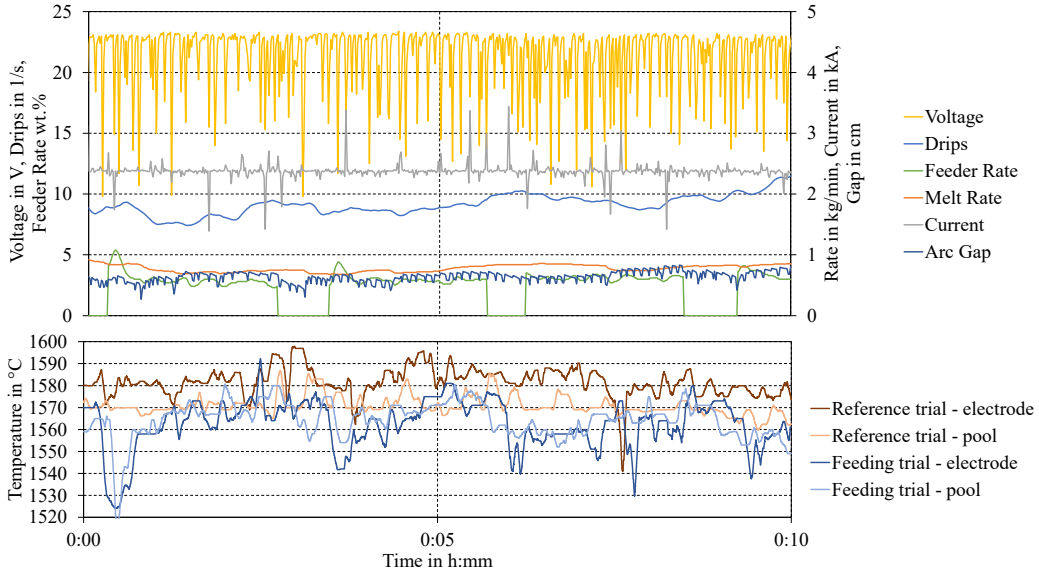

Figure 6: Excerpt of melt protocol for the remelting trial with loose powder feeding (top) and temperatures from IR imager for the reference trial without powder feeding and the trial with powder feeding (bottom) in scenario B during main melting phase.

4. Conclusion

Two trial setups have been presented in order to demonstrate the feasibility of metal powder addition during consumable VAR. The limitation tests in scenario A showed the upper limits for powder addition on a macroscopic level with large areas of undissolved powder and porosity, making the produced ingots useless for further industrial application. However, it was also shown that material is well distributed over the entire pool if agglomeration of particles is avoided while feeding. The principle could be used for the addition of smaller quantities of alloying elements during remelting making it a tool to homogenize chemical composition in an ingot with a concentration gradient over ingot length. Concerns regarding operation safety cannot be eliminated completely after this preliminary testing, but dangerous arc modes contradicting material feeding in general were not observed during furnace operation. Trials in scenario B showed promising results regarding the alteration of macroscopic columnar solidification towards a more upwards oriented grain structure, indicating a cooling effect by the material addition. This phenomenon has also been indicated by IR thermography results. Other than the intentionally provided horizontal cracks, the powder addition did not create large scale visible defects. Since the results in scenario B are based on only two comparable trials, validation testing, other energy input parameters, materials and a wider range of powder addition amounts are needed to confirm the above-mentioned results and benefits of metal powder addition during VAR. To ensure ingot quality a microstructure analysis and mechanical testing is advised for future work.

Acknowledgements

This research was funded by the german Federal Ministry of Education and Research, grant number: 03HY111E

References

[1] Zhao Xiaohua, Sun Feng, Wang Kaixuan, Liu Peng, He Yongsheng, Wu Wei, Luo Wenzhong and Liu Xianghong Preparation method for improving component uniformity of large-size titanium alloy ingot *CN111519066B*

[2] Huang Shuo, Zhao Guangpu, Zhang Beijiang, Duan Ran, Qin Heyong, Li Lianpeng, Chou Yingyu and Qi Chao Smelting process of high-niobium high-temperature alloy large-size ingot and high-niobium high-temperature alloy large-size ingot *CN111876649B*

[3] Bernd Spaniol, Stefan Csirka, Mark and Markus Schultheis Method for the melt-metallurgical representation of intermetallic compound nb3sn *EP3489373A1*

[4] Schuyler A. Herres and James A Davis Electric apperatus for melting refractory metals *US2541764A*

[5] Al'tman Petr Semenovich, Smirnov Vladimir Grigor'evich and Chechulin Sergej Mikhajlovich Consumable electrode for vacuum arc furnace and method of making it *RU2359432C1*

[6] Al'tman Petr Semenovich, Maksimov Aleksandr Jur'evich and Bachurin Vladimir Andreevich Ingot melting method *RU2304176C2*

[7] Al'tman Petr Semenovich Method for providing explosion safety at operation of vacuum arc furnace for smelting of reaction metal ingots *RU2403298C2*

[8] Al'tman Petr Semenovich, Goncharov Anatolij Egorovich, Medinets Sergej Viktorovich, Shamro Pavel Vladimirovich and Makoveev Dmitrij Valentinovich Method of control of interelectrode space during vacuum arc melting *RU2374337C1*

[9] Al'tman Petr Semenovich, Goncharov Anatolij Egorovich, Medinets Sergej Viktorovich, Shamro Pavel Vladimirovich and Makoveev Dmitrij Valentinovich Method of control of vacuum arc melting process *RU2375473C1*

[10] Al'tman Petr Semenovich, Smirnov Nikolaj Vasil'evich and Bachurin Vladimir Andreevich Method of control over vacuum arc fusion *RU2324748C2*

[11] Al'tman Petr Semenovich Method of securing explosion safety at operation of vacuum arc furnace for production of ingots out of reactive metals *RU2337157C2*

[12] Al'tman Petr Semenovich and Goncharov Anatolij Egorovich Arc furnace consumable electrode *RU2356188C1*

[13] Al'tman Petr Semenovich and Goncharov Konstantin Alekseevich Melting method of bars in vacuum arc furnace *RU2323985C2*

[14] Al'tman Petr Semenovich and Matveev Vladimir Afanas'evich Method of preparation of consumable electrode *RU2374338C1*

[15] Al'tman Petr Semenovich and Tashkinov Aleksej Jur'evich Method for controlling of vacuum arc-melting process *RU2278176C1*

[16] Betsy J. Bond, Laurence A. Jackman and A. Stewart Ballantyne Method for producing large diameter ingots of nickel base alloys *WO2002072897A1*

[17] Christopher L. Hysinger, Joseph J. Beaman, David Melgaard and Rodney L. Williamson Multiple input electrode gap controller *US5930284A*

[18] Cihangir Demirci and Jutta Klöwer Method for producing composite metal semi-finished products *WO2010037355A1*

[19] David R. Mathews and Robert J. Krieger Electric arc melting apparatus and associated method *US4581745A*

[20] Du Yaning, Peng Changhu, Li Huiwu, Wang Jinqun, Lan Xianhui, Fangxiang Ming, Ren Yuan, Liu Jun and Liu Haiming Automatic arcing device for vacuum consumable electric-arc furnace and control method *CN103045877B*

[21] Du Yaning *et al* For the refrigerating unit of vacuum consumable electrode arc furnace water jacket type crystallizer *CN204058565U*
[22] Frank J. Zanner, Rodney L. Williamson and Mark F. Smith Metals purification by improved vacuum arc remelting *US5373529A*
[23] Goncharov Anatolij Egorovich and Puzakov Igor' Jur'evich Procedure for ingot vacuum-arc melting *RU2425157C2*
[24] Gorbatjuk Aleksandr Fedorovich, Goncharov Anatolij Egorovich, Puzakov Igor' Jur'evich, Medinets Sergej Viktorovich, Shamro Pavel Vladimirovich and Makoveev Dmitrij Valentinovich Procedure for control and stabilisation of inter-electrode space *RU2425156C2*
[25] He Tao *et al* Electrode block structure for inhibiting welding line from dropping block in smelting process *CN215682680U*
[26] Helmut Grof, Uwe Reimpell and Anton Wamser Electrode clamping device for electroremelting plants *US4339624A*
[27] Hua Zhengli, Luo Wenzhong, Wu Jiangtao, Wang Longzhou, Wang Kaixuan and Liu Xianghong Arc-extinguishing process of VAR titanium alloy primary ingot *CN110964932A*
[28] Hua Zhengli, Luo Wenzhong, Wu Ming, Wang Kaixuan, Liu Xianghong and Feng Yong Cooling method of titanium alloy ingot *CN110904341A*
[29] Hua Zhengli, Wang Kang, He Yongsheng, He Tao, Sun Feng, Du Yujun, Wang Kaixuan, Liu Xianghong, Feng Yong and Zhang Pingxiang Smelting method for improving bottom quality of VAR titanium alloy primary ingot *CN113088719A*
[30] Ivaylo Popov, Lothar Lippert, Stefan Lemke and Thomas Kilzer Remelting plant for metals, and method for remelting metals *WO2022223208A1*
[31] Ivaylo Popov, Jens Hofmann and Michael Mutz Umschmelzanlage *DE 10 2016 100 372 A1*
[32] Ivaylo Popov, Lothar Lippert, Stefan Lemke and Thomas Kilzer Umschmelzanlage für Metalle *DE 10 2021 109 823 B3*
[33] Ivaylo Popov and Ulrich Bibricher Remelting plant and method for operating a remelting plant *EP3752303B1*
[34] John Veil Consumable electrode remelting furnace and method *US4569056A*
[35] Katsuichi Takahash and Shigeo Anpo Manufacture of high purity titanium material, and multistage melting method of titanium ingot *JPH1025527A*
[36] KenJi Suzuki Method for manufacturing titanium ingot *JP2007162071A*
[37] KenJi Suzuki Method for producing titanium ingot using vacuum arc melting furnace *JP2010116581A*
[38] Kondrashov Evgenij Nikolaevich, Maksimov Aleksandr Yurevich, Konovalov Lev Vladimirovich, Gorina Aleksandra Vladimirovna, Klimov Sergej Mikhajlovich and Leder Mikhail Ottovich Method for vacuum arc final remelting of titanium alloy ingots of vt3-1 brand *RU2749010C1*
[39] Konovalov Lev Vladimirovich, Kondrashov Evgenij Nikolaevich, Maksimov Aleksandr Jur'evich, Fedorov Nikolaj Semenovich and Puzakov Igor' Jur'evich Procedure for control of spark gap during vacuum arc melting and facility for implementation of this procedure *RU2395596C2*
[40] Lee A. Bertram, Rodney L. Williamson, David Melgaard, Joseph Beaman and David G. Evans Dynamic control of remelting processes *US6115404A*
[41] Lei Qiang, Zhu Junli, Fan Yanjie, He Tao, Luo Wenzhong, Wang Longzhou and Xiao Qi Welding method for eliminating titanium and titanium alloy consumable electrode weld cracks *CN112338331A*
[42] Li Huiwu, Peng Changhu, Ren Yuan, Wang Jinqun, Lan Xianhui, Du Yaning, Zhang Jia, Xiang Ming, Wen Huafeng and Zhang Lei Water-cooled furnace chamber used for vacuum arc remelting furnace *CN103225950A*
[43] Li Junren, Liu Jun, Luo Wenzhong, Peng Changhu, Ye Mingjun, Guo Ruibo and Li Yang A kind of adjustable crucible cleaning brush *CN206500410U*

[44] Li Junren, Du Jianchao, Liu Jun, Wang Xiaocheng, Fu Baoquan, Luo Wenzhong and Yang Bin A kind of consumable electrode vacuum furnace titanium or titanium alloy electrode and preparation method thereof *CN107619942A*
[45] Li Junren, Peng Changhu, Liu Jun, Fu Baoquan, Sun Dong, Qi Yili and Luo Wenzhong: Feng Yi Crucible for vacuum consumable arc furnace *CN104613749A*
[46] Liu Peng, He Tao, Pan Yanjie, Sun Zhizhong, He Yongsheng, Luo Wenzhong and Liu Xianghong Method for recycling scrapped titanium alloy auxiliary electrode *CN113355514A*
[47] Liu Peng, Zhao Xiaohua and Hua Zhengli Method for welding titanium alloy ingot casting in furnace *CN111014877A*
[48] Liu Xianghong *et al* Brass crucible thick bottom pad and crucible for vacuum consumable arc melting *CN219656580U*
[49] Liu Xianghong, Wu Jiangtao, He Yongsheng, He Tao, Hua Zhengli, Yang Ce and Feng Xiaofei Low-cost short-process recovery method for titanium and titanium alloy residues *CN115449654A*
[50] Liu Xianghong, Wu Yulun, Shang Jinjin, Zhong Nanjing, Du Yujun, Wang Kaixuan, Li Shaoqiang, Du Yushen and Feng Yong Method for controlling depth of variable-section titanium alloy VAR electrode molten pool *CN116751978A*
[51] Liu Xianghong *et al* Method for eliminating welding adhesion in titanium alloy ingot furnace *CN116511645A*
[52] Liu Xianghong, Shang Jingjing, He Yongsheng, Yang Ce, Ma Fanjiao, Yang Hui, Hou Fengqi and Wang Kaixuan Method for improving stability of titanium-niobium alloy in smelting process *CN114250368A*
[53] Liu Xianghong *et al* Method for recycling titanium alloy cast ingot and removing scraps in whole process *CN116814998A*
[54] Liu Xianghong, Zhang Tongtong, Wang Kang, Shang Jinjin, Wang Kaixuan, Li Shaoqiang, Du Yushen and Feng Yong Preparation method of large-size low-oxygen-content TiAl alloy cast ingot *CN116770087A*
[55] Liu Xianghong, Shang Jinjin, He Yongsheng, Yang Ce, Du Yuxiang, Zhang Pingxiang, Feng Yong and Fu Baoquan Preparation method of titanium-niobium alloy ingot *CN115029570A*
[56] Liu Xianghong *et al* VAR smelting method for preparing full-columnar crystal titanium alloy ingot *CN113061761A*
[57] Liu Xianghong *et al* VAR smelting method for preparing large-size easily-segregated titanium alloy ingot in strong cooling mode *CN113186406A*
[58] Luke Borkowski and Alexander Staroselsky Vacuum arc remelting (var) processing *EP3799971A1*
[59] Luo Wenzhong *et al* Control method for preventing block dropping at welding seam position after VAR primary ingot smelting *CN114293042A*
[60] Mark Gilbert Benz, Michael Francis Henry, William Thomas Carter JR. and Bernard Patrick Bewlay Vacuum arc remelting apparatus and process *EP1184470B1*
[61] Masaaki Koizumi, Nobuo Hiroyuki and Okano Fukada Consumable electrode for production of Nb-Ti alloys *US4612040A*
[62] Matthias Achtermann, Willy Fuerwitt, Volker Guether and Hans-Peter Nicolai Method for the production of a β-γ-TiAl base alloy *US8668760B2*
[63] Matthias Blum, Georg Jarczyk, Anita Chatterjee, Willy Fuerwitt, Volker Guether, Helmut Clemens, Heinz Danker, Reiner Gerling, Friedhelm Sasse and Frank-Peter Schimanski Method for producing alloy ingots *WO200304189 6A2*
[64] Meiji Watanabe and Satoshi Sugawara Manufacturing method of electrode for melting titanium alloy *JP20180626 96A*
[65] Osamu Tada, Satoshi Sugawara, Yoshihiro Hatsuta and Takeshi Shinraki Consumable electrode *JP3865642B2*
[66] Otto Stenzel Method and device for the compensation of the influence of the weight of a conductor of current supply on a weighing apparatus *EP0212491B1*

[67] Puzakov Igor Yurevich, Klimov Sergej Mikhajlovich, Suslov Aleksej Valerievich and Ermokhin Pavel Gennadievich Method for vacuum arc remelting of ingots from manganese-alloyed titanium alloys *RU2763827C1*
[68] Ralf Oehler, Harald Scholz and Frank-Werner Hoffmann Device and method for filtering supply network failures out from an electrode signal in a metallurgical electro remelting method *WO201205230 3A1*
[69] Ralf Oehler, Harald Scholz and Frank-Werner Hoffmann Method and device for closed-loop control of the electrode gap in a vacuum arc furnace *US9538587B2*
[70] Ralf Oehler and Ivaylo Popov Re-melting furnace and universal joint, in particular for the electrode rod mounting of a re-melting furnace *WO201417712 9A2*
[71] Ralf Oehler and Ivaylo Popov Smelting furnace and universal joint for the electrode rod mounting of a smelting furnace *EP2992287B1*
[72] Ramesh S. Minisandram Systems and methods for forming and processing alloy ingots *US9533346B2*
[73] Raymond Roberts Automatic melt rate control system for consumable electrode remelting *US4131754A*
[74] Raymond Roberts Method and apparatus for controlling electrode drive speed in a consumable electrode furnace *EP0042689B2*
[75] Raymond Roberts Purification of a metalloid by consumable electrode vacuum arc remelt process *WO2013032703A2*
[76] Rodney L. Williamson, Frank J. Zanner and Stephen M. Grose Arc voltage distribution skewness as an indicator of electrode gap during vacuum arc remelting *US5708677A*
[77] Rodney L. Williamson, Frank J. Zanner and Stephen M. Grose Controlling electrode gap during vacuum arc remelting at low melting current *US5621751A*
[78] Rodney L. Williamson, David Melgaard and Joseph Beaman Pool power control in remelting systems *US8077754B1*
[79] Rodney L. Williamson and Joseph Beaman Ingot solidification controller for vacuum arc remelting *US9220131B1*
[80] Rodney Wiliamson, David Melgaard and Joseph Beaman Apparatus to control the total energy flux into the top ingot surface during vacuum arc remelting processes *US10422584B2*
[81] Shang Jinjin, Zhao Xiaohua, Lei Qiang, Liu Xianghong, Zeng Weidong, He Yongsheng, Liang Jingfan and Sun Zhizhong Method for improving surface quality of titanium alloy ingot *CN115747543A*
[82] Takeshi Sugita, Masayuki Ichikawa and Hirotaka Kashiwazaki Consumable electrode type arc melting furnace *JP6953256B2*
[83] Takeshi Sugita, Masayuki Ichikawa and Hirotaka Kashiwazaki Operation method of consumable electrode type arc melting furnace, and consumable electrode type arc melting furnace *JP2019059970A*
[84] Tetjukhin Vladislav Valentinovich, Levin Igor' Vasil'evich, Puzakov Igor' Jur'evich and Fedotov Oleg Germanovich Consumable electrode producing method *RU2313590C1*
[85] Tetjukhin Vladislav Valentinovich, Gorbatjuk Aleksandr Fedorovich, Puzakov Igor' Jur'evich, Kiselev Nikolaj Vladimirovich, Klimov Mikhail Ivanovich and Klimov Sergej Mikhajlovich Method to control electric arc during vacuum-arc remelting *RU2536561C1*
[86] Tetjukhin Vladislav Valentinovich and Ivanov Aleksandr Valentinovich Method of obtaining soliol ingots-electrodes *RU2386707C1*
[87] Tong Puchao, Sheng Bin, Chen Qiang, Zhang Lan, Cao Yike, Liu Jun, Li Zhaokai, Tang Xiaodong, Jing Huiqing and Luo Wenzhong Electrode rod insulation detection device of vacuum consumable arc furnace *CN219715646U*
[88] Vladislav Valentinovich Tetyukhin and Igor Vasilievich Levin Method for melting a pseudo beta-titanium alloy comprising (4.0-6.0)% al - (4.5-6.0)% mo - (4.5-6.0)% v - (2.0-3.6)% cr, (0.2-0.5)% fe - (0.1-2.0)% zr *EP2623620B1*

[89] Wu Jiangtao, Hua Zhengli, Wu Ming, Shang Jinjin, Li Junren, He Yongsheng and Luo Wenzhong Crucible for VAR refractory alloy *CN214120754U*
[90] Wu Ming, Hua Zhengli, Liang Jingfan and Liu Peng Method for improving visibility and stability of titanium alloy in argon-filling smelting process *CN113174501A*
[91] Xia Yong, Shang Jinjin, He Li, Zhao Genan, Wang Yangyang, He Tao, He Yongsheng, Peng Changhu, Liu Xianghong and Feng Yong Copper crucible for vacuum consumable or non-consumable electric arc furnace *CN216049121U*
[92] Yoshihiro Hatsuta, Takeshi Shinraki and Osamu Tada Consumable electrode for melting alloy ingot, and its producing method *JP2004263217A*
[93] Zhang Huijie, Shang Jinjin, Yang Ce, Fu Jie, Liu Xianghong, Du Yuyi and Feng Yong NbTaHf alloy ingot and preparation method thereof *CN115747597A*
[94] Zhang Lan, Qi Yili, Chen Qiang, Cao Yike, Sheng Bin, Tong Puchao, Li Zhaokai and Luo Wenzhong Dismounting device for dynamic seal of vacuum consumable arc furnace *CN219901977U*
[95] Zhang Pingxiang, Feng Yong, Liu Xianghong, Shang Jinjin, Fu Baoquan and He Yongsheng Preparation method of high-uniformity NbTi alloy ingot *CN113005314A*
[96] Specht A and Friedrich B 2023 Challenges and Opportunities of Thermography in Metallurgy *Proceedings of the 62nd Conference of Metallurgists, COM 2023 Conference of Metallurgists* 1st edn (Cham: Springer Nature Switzerland; Imprint Springer) pp 285–95